Live imaging of neurogenesis in the adult mouse hippocampus

Gregor-Alexander Pilz[1*], Sara Bottes[1*], Marion Betizeau[1,3], David J. Jörg[4], Stefano Carta[1,2], Benjamin D. Simons[4], Fritjof Helmchen[2], Sebastian Jessberger[1#]

[1]Laboratory of Neural Plasticity and [2]Laboratory of Neural Circuit Dynamics, Faculties of Medicine and Science, Brain Research Institute, University of Zurich, 8057 Zurich, Switzerland. [3]Institute of Neuroinformatics, University of Zurich and Swiss Federal Institute of Technology (ETH) Zurich, 8057 Zurich, Switzerland. [4]Cavendish Laboratory, Department of Physics, University of Cambridge, Cambridge CB3 0HE, UK; Wellcome Trust/Cancer Research UK Gurdon Institute, University of Cambridge, Cambridge CB2 1QN, UK; Wellcome Trust-Medical Research Council Cambridge Stem Cell Institute, University of Cambridge, Cambridge CB2 1QR, UK. [*]These authors contributed equally. [#]Correspondence to: jessberger@hifo.uzh.ch

Neural stem/progenitor cells (NSPCs) generate neurons throughout life in the mammalian hippocampus. We used chronic *in vivo* imaging and followed genetically labeled individual NSPCs and their progeny in the mouse hippocampus for up to 2 months. We show that NSPCs targeted by the endogenous Achaete-scute homolog 1 (Ascl1)-promoter undergo limited rounds of symmetric and asymmetric divisions, eliciting a burst of neurogenic activity, after which they are lost. Further, our data reveal unexpected asymmetric divisions of non-radial glia-like NSPCs. Cell fates of Ascl1-labeled lineages suggest a sequential transition from a proliferative to a neurogenic phase, reminiscent of a developmental-like program. By providing a comprehensive description of lineage-relationships, from dividing NSPCs to newborn neurons integrating into the hippocampal circuitry, our data provide insight into how NSPCs support life-long hippocampal neurogenesis.

One Sentence Summary: Direct observation of single hippocampal stem cells catches them in action.

The hippocampus requires new neurons in the dentate gyrus (DG) throughout life for learning and memory (*1*). Failing or altered hippocampal neurogenesis has been implicated in a variety of diseases such as major depression and age-related cognitive decline (*2, 3*). Based on thymidine analogue labeling, *in vivo* lineage tracing and cell ablation studies it has been proposed that radial glia-like (R) neural stem/progenitor cells (NSPCs) represent the *bona fide* stem cells of the adult DG (*4-9*). According to the prevailing model of adult hippocampal neurogenesis, R cells self-renew - here defined as generating a daughter cell with equivalent molecular characteristics and potency - and give rise to proliferative non-radial glia-like cells (NR cells) that divide symmetrically to generate granule cells (*3*). However, the self-renewal capacity and lineage-relationships of R cells remain controversial due to the lack of longitudinal observations of individual R cells and their progeny within their niche (*7, 8*). Similar to previous imaging approaches probing the dynamics of somatic stem cell behavior in the non-vertebrate nervous system and other stem cell niches (*10-17*), we here used chronic *in vivo* imaging to track the fate of individual R cells over time within the adult DG.

To label hippocampal R cells we used mice expressing a Tamoxifen (Tam)-regulable Cre recombinase under the control of the endogenous Achaete-scute homolog 1 (Ascl1) promoter crossed with a tdTomato reporter mouse line (Ascl1-tdTomato mice) (*18*). Ascl1-expressing cells represent an essential population of NSPCs in the adult DG (*18-20*). Adult Ascl1-tdTomato mice were implanted with a cortical window leaving the

hippocampal formation intact and allowing for 2-photon imaging (Fig. 1A and Fig. S1A) (*21*). A single Tam injection induced sparse labeling of Ascl1-expressing cells that were classified as R and NR cells based on morphological features and marker expression (Fig. 1B, C, Fig. S2 and Movie S1). Only R cells were analyzed as a starting population. Individual clones were imaged approximately every 12-24 hours (unless otherwise indicated) and followed for up to 2 months (Fig. 1D, E and Fig. S3). Imaged clones (n = 63) were characterized based on behavioral and morphological criteria (see Methods, Fig. S2, Movie S2 and Table S1), allowing for the construction of individual lineage trees (Fig. 1E, Fig. S3 and Movie S3). After imaging, the final fate of progeny was confirmed using immunohistochemistry (Fig. 1E, F and Fig. S4).

In agreement with previous static clonal lineage tracing experiments, we found that in 8-9 weeks-old Ascl1-tdTomato mice 67% (42/63) of R cells entered cell cycle and became active during the time course of imaging. Out of these active R cells 88% (37/42) divided within the first 20 days and, as a population, gave rise to both neuronal and glial daughter cells (Fig. 1D-F and Figs. S3, S4A-D) (*19*).

Once activated, cycling R cells divided 2.3 ± 0.1 times on average and persisted for 9.6 ± 1.4 days (Fig. 2A and Fig. S3). We did not find Ascl1-targeted R cells that generated neuronal progeny and returned to long-term (> 3 weeks) quiescence within the 2 months observational period in all analyzed clones (Figs. S3, S4E). This suggests that, once activated, Ascl1-targeted R cells do not re-enter long-term quiescence, but generate a burst of neurogenic activity before committing to terminal neuronal differentiation and loss (Fig. 2A and Figs. S3, S4E-H). The average clone size derived from active R cells was 4.8 ± 0.5 cells (Fig. 2B and Fig. S3). We found no evidence for terminal

differentiation of R cells into astrocytes, which had been suggested for nestin-expressing NSPCs after several rounds of cell division (*8*) (Figs. S3, S4H). Thus, self-renewal capacity of Ascl1-targeted R cells is temporally limited, similar to previous results obtained using population-based static analysis of nestin-labeled NSPCs (*8*).

We then turned to consider the fate behavior of activated R cells and their progeny. Previously, it has been proposed that the predominant mode of R cell division is asymmetric (*6-8, 22*). However, without access to continuous *in vivo* cell tracking, evidence for asymmetric fate has been indirect. Morphological analyses of cell body and radial glia-like processes of R cells before and after cell division revealed that the morphology of R cells remained stable (Fig. 2C, D and Fig. S5A), providing direct evidence for asymmetric cell divisions (*6-8, 22*). While the majority of observed first cell divisions were asymmetric, generating a R cell and a NR cell (79.3%, Fig. 2E, F), we found that 13.8% of first R cell divisions expanded the R cell pool via symmetric divisions (Fig. 2E, G), mirroring the behavior found in static clonal studies of R cells targeted by a nestin promoter (*7*). With the further identification of direct neurogenic cell divisions of R cells (Fig. 2E and Figs. S3, S5B, C), all three modes of division were observed, reminiscent of the fate behavior described for NSPCs in the developing neocortex (*23, 24*). The majority (70.6%) of all R cell divisions led to the generation of NR cells that were identified based on the lack of a radial process, their ability to enter the cell cycle, and to generate neuronal progeny at later stages during the imaging period (Fig. 2E, F). In contrast to previously suggested models (*3*), we found not only symmetric, neurogenic cell divisions of NR cells but also a substantial fraction (24.2% of all NR divisions) of asymmetric cell divisions, yielding one renewed NR cell and one neuronal

daughter cell (Fig. 2H-J) (*9*). NR cells underwent as many as 6 rounds of cell divisions (with an average of 2.9 ± 0.2 divisions); thus, NR cells represent a major source of clonal expansion (Fig. 2H-J and Fig. S3).

Chronic imaging also allowed us to analyze whether division times (T_D) are correlated with previous cell divisions, or within clonally related lineages. We analyzed the T_D of R and NR divisions and found that, once activated, the T_D of R and NR cells remained constant (Fig. 2K). T_D times of sister cells were correlated among R cell daughters, while no correlation was detected for daughters of NR cells (Fig. 2L, M), suggesting segregation of cellular features selectively in R cells that determine the daughter cells' re-entry into cell division.

Not all newborn cells survive and become stably integrated into the DG circuitry. Two critical periods of cell death have been described previously: one early phase of cell death within the first days after cell birth and a later phase of neuronal selection that is activity-dependent and occurs approximately 1-3 weeks after new neurons are born (*25-27*). Consistent with previous reports, we found an average frequency of cell death among the progeny per lineage of 59.6% and identified two waves of cell death occurring around 1-4 days and 13-18 days after birth, respectively (Fig. 3A, B) (*25-27*). We identified inter-clonal variability with some clones showing no cell death whereas other clones completely disappeared over time (Fig. 3A). Furthermore, we found differences regarding the susceptibility for cell death among individual sub-lineages when analyzing levels of early cell death (until 7 days after cell birth; Fig. 3C-F), suggesting that cell death is not evenly distributed among progeny. The underlying cause for the observed subtree-associated variability of cell death remains unknown, but may involve intrinsic

mechanisms – for example retrotransposon-associated genetic alterations or unequal segregation of aging factors (*28, 29*) – rather than environmental, niche-dependent factors, e.g., growth factor availability (*3*). Supporting this interpretation, we found that surviving cells can lie interspersed among death-prone cells (Fig. 3G).

Inspection of reconstructed R cell lineages revealed a wide variability of neurogenic potential and fate outcomes (Fig. S3). Following induction, some R cells differentiated early, giving rise to one or two short-lived neurons, while others gave rise to more than 10 surviving neurons (Fig. 2B, Fig. S3, S4F). Despite this variability, some features of R cell fate behavior were conserved among all lineage trees. In particular, we found no instance of an asymmetrical R cell division being followed by a symmetric R cell duplication (Fig. 2E and Fig. S3) suggesting that, once activated, either R cells move sequentially from a symmetrically to an asymmetrically dividing phase, or that the proliferative potential of R cells becomes progressively exhausted so that symmetrical duplicative divisions become increasingly scarce. By contrast, variability in the output of dividing NR cells was indicative of a conserved pattern of stochastic fate, with NR cells choosing between symmetric duplication, asymmetric division and symmetric differentiation with probabilities independent of the cell generation (Fig. 2H and Fig. S3).

Thus, based on these observations, we considered the quantitative fate behavior of R cells. Given the sequential pattern of symmetric and asymmetric divisions, we questioned whether R cells might be following a developmental-like program, switching irreversibly from a phase of proliferative (symmetrical) divisions to a phase of neurogenic (asymmetrical) divisions, as observed during cortical development (Fig. 4A, Fig. S6A, Table S2) (*30*). Using a statistical modelling approach, we assessed quantitatively the

viability of this hypothesis by fitting the lengths of putative proliferative and neurogenic phases against average clonal properties (see Methods). This simple developmental-like paradigm yielded predictions on the proliferative output, the cell fate distributions and the average clonal composition over time that were in agreement with the observed data within the theoretically predicted variability (Fig. 4B–D, Methods). As a consistency check, we also assessed whether the observed sequential fate pattern could represent the chance outcome of stochastic fate behavior, with R cells becoming progressively biased away from self-renewal towards differentiation over time (Figs. S6, S7). However, given the observed cell fate frequencies and the number of observed lineage trees, we estimated the chance for such an outcome to be only 2.4% (see Methods). Thus, we conclude that a model in which the sporadic entry of R cells into cycle activates a developmental-like program of fate, leading to a burst of neurogenic activity, provides the most plausible explanation of the lineage data.

We used chronic imaging of individual R cells and their progeny to characterize the cellular dynamics underlying adult hippocampal neurogenesis. Our data show that, following activation, Ascl1-targeted R cells enter a developmental-like program, leading to a burst of neurogenic activity. However, self-renewal is temporally limited, as we did not observe repeated shuttling between quiescence and proliferation, leading to a loss of activated R cells. These findings do not rule out the previously reported presence of NSPCs in the mammalian DG that shuttle back and forth between quiescent and activity, dividing for extended periods (*7, 31, 32*). NSPC heterogeneity has been postulated and the Ascl1-targeted population analyzed here may not include all subtypes that are capable of generating neuronal progeny in the adult DG (*33-35*). Previous data suggested that

approximately 10-15% of all granule cells are adult-generated in the mouse hippocampus. This indicates that adult NSPCs generate 30'000 to 45'000 granule cells during the entire lifespan (*5, 36, 37*), which, as a fraction, appears to be lower in the rodent compared to the human DG (*38*). We found that, once activated, individual Ascl1-targeted R cells generated 4.8 neurons on average. Based on previous estimates that the DG contains approximately 10'000 R cells in 2 month-old mice (*8*), the total number of cells that can be generated by Ascl1-targeted cells with the principles of clone expansion described here (approx. 45'000) appears to be sufficient to explain a substantial part of hippocampal neurogenesis. Using *in vivo* imaging our results elucidate the cellular dynamics of physiological adult neurogenesis and lay the basis to understand the molecular mechanisms governing the steps from dividing stem cells to newborn neurons.

References:

1. C. Anacker, R. Hen, Adult hippocampal neurogenesis and cognitive flexibility - linking memory and mood. *Nature reviews* **18**, 335-346 (2017).
2. S. Yun, R. P. Reynolds, I. Masiulis, A. J. Eisch, Re-evaluating the link between neuropsychiatric disorders and dysregulated adult neurogenesis. *Nature medicine* **22**, 1239-1247 (2016).
3. J. T. Goncalves, S. T. Schafer, F. H. Gage, Adult Neurogenesis in the Hippocampus: From Stem Cells to Behavior. *Cell* **167**, 897-914 (2016).
4. D. C. Lagace *et al.*, Dynamic contribution of nestin-expressing stem cells to adult neurogenesis. *J Neurosci* **27**, 12623-12629 (2007).

5. I. Imayoshi *et al.*, Roles of continuous neurogenesis in the structural and functional integrity of the adult forebrain. *Nat Neurosci*, (2008).

6. B. Seri, J. M. Garcia-Verdugo, B. S. McEwen, A. Alvarez-Buylla, Astrocytes give rise to new neurons in the adult mammalian hippocampus. *J Neurosci* **21**, 7153-7160. (2001).

7. M. A. Bonaguidi *et al.*, In Vivo Clonal Analysis Reveals Self-Renewing and Multipotent Adult Neural Stem Cell Characteristics. *Cell* **145**, 1142-55 (2011).

8. J. M. Encinas *et al.*, Division-coupled astrocytic differentiation and age-related depletion of neural stem cells in the adult hippocampus. *Cell Stem Cell* **8**, 566-579 (2011).

9. S. Lugert *et al.*, Quiescent and active hippocampal neural stem cells with distinct morphologies respond selectively to physiological and pathological stimuli and aging. *Cell Stem Cell* **6**, 445-456 (2010).

10. J. S. Barbosa *et al.*, Live imaging of adult neural stem cell behavior in the intact and injured zebrafish brain. *Science* **348**, 789-793 (2015).

11. D. B. Gurevich *et al.*, Asymmetric division of clonal muscle stem cells coordinates muscle regeneration in vivo. *Science* **353**, aad9969 (2016).

12. P. Rompolas, K. R. Mesa, V. Greco, Spatial organization within a niche as a determinant of stem-cell fate. *Nature* **502**, 513-518 (2013).

13. P. Rompolas *et al.*, Live imaging of stem cell and progeny behaviour in physiological hair-follicle regeneration. *Nature* **487**, 496-499 (2012).

14. P. Rompolas *et al.*, Spatiotemporal coordination of stem cell commitment during epidermal homeostasis. *Science* **352**, 1471-1474 (2016).

15. C. Lo Celso *et al.*, Live-animal tracking of individual haematopoietic stem/progenitor cells in their niche. *Nature* **457**, 92-96 (2009).

16. Y. Xie *et al.*, Detection of functional haematopoietic stem cell niche using real-time imaging. *Nature* **457**, 97-101 (2009).

17. L. Ritsma *et al.*, Intestinal crypt homeostasis revealed at single-stem-cell level by in vivo live imaging. *Nature* **507**, 362-365 (2014).

18. E. J. Kim, J. L. Ables, L. K. Dickel, A. J. Eisch, J. E. Johnson, Ascl1 (Mash1) defines cells with long-term neurogenic potential in subgranular and subventricular zones in adult mouse brain. *PLoS ONE* **6**, e18472 (2011).

19. G. J. Sun *et al.*, Tangential migration of neuronal precursors of glutamatergic neurons in the adult mammalian brain. *PNAS* **112**, 9484-9489 (2015).

20. J. Andersen *et al.*, A transcriptional mechanism integrating inputs from extracellular signals to activate hippocampal stem cells. *Neuron* **83**, 1085-1097 (2014).

21. G. A. Pilz *et al.*, Functional Imaging of Dentate Granule Cells in the Adult Mouse Hippocampus. *J Neurosci* **36**, 7407-7414 (2016).

22. H. K. Suh *et al.*, In Vivo Fate Analysis Reveals the Multipotent and Self-Renewal Capacities of Sox2+ Neural Stem Cells in the Adult Hippocampus. *Cell Stem Cell* **1**, 515-528 (2007).

23. J. H. Lui, D. V. Hansen, A. R. Kriegstein, Development and evolution of the human neocortex. *Cell* **146**, 18-36 (2011).

24. M. Gotz, W. B. Huttner, The cell biology of neurogenesis. *Nature reviews. Molecular cell biology* **6**, 777-788 (2005).

25. G. Kempermann, D. Gast, G. Kronenberg, M. Yamaguchi, F. H. Gage, Early determination and long-term persistence of adult-generated new neurons in the hippocampus of mice. *Development* **130**, 391-399 (2003).

26. A. Sierra *et al.*, Microglia shape adult hippocampal neurogenesis through apoptosis-coupled phagocytosis. *Cell Stem Cell* **7**, 483-495 (2010).

27. A. Tashiro, V. M. Sandler, N. Toni, C. Zhao, F. H. Gage, NMDA-receptor-mediated, cell-specific integration of new neurons in adult dentate gyrus. *Nature* **442**, 929-933 (2006).

28. D. L. Moore, G. A. Pilz, M. J. Arauzo-Bravo, Y. Barral, S. Jessberger, A mechanism for the segregation of age in mammalian neural stem cells. *Science* **349**, 1334-1338 (2015).

29. A. R. Muotri *et al.*, Somatic mosaicism in neuronal precursor cells mediated by L1 retrotransposition. *Nature* **435**, 903-910 (2005).

30. P. Gao *et al.*, Deterministic progenitor behavior and unitary production of neurons in the neocortex. *Cell* **159**, 775-788 (2014).

31. G. Kempermann, The pessimist's and optimist's views of adult neurogenesis. *Cell* **145**, 1009-1011 (2011).

32. N. Urban *et al.*, Return to quiescence of mouse neural stem cells by degradation of a proactivation protein. *Science* **353**, 292-295 (2016).

33. M. A. Bonaguidi, J. Song, G. L. Ming, H. Song, A unifying hypothesis on mammalian neural stem cell properties in the adult hippocampus. *Current opinion in neurobiology* **22**, 754-761 (2012).

34. Z. Chaker, P. Codega, F. Doetsch, A mosaic world: puzzles revealed by adult neural stem cell heterogeneity. *Wiley Interdiscip Rev Dev Biol* **5**, 640-658 (2016).

35. N. A. DeCarolis *et al.*, In vivo contribution of nestin- and GLAST-lineage cells to adult hippocampal neurogenesis. *Hippocampus* **23**, 708-719 (2013).

36. G. Kempermann, H. G. Kuhn, F. H. Gage, Genetic influence on neurogenesis in the dentate gyrus of adult mice. *PNAS* **94**, 10409-10414 (1997).

37. J. Ninkovic, T. Mori, M. Gotz, Distinct modes of neuron addition in adult mouse neurogenesis. *J Neurosci* **27**, 10906-10911 (2007).

38. K. L. Spalding *et al.*, Dynamics of hippocampal neurogenesis in adult humans. *Cell* **153**, 1219-1227 (2013).

Acknowledgments: The data reported are presented in the main paper and the supplementary materials (Figures S1-S7, Movies S1-S3, Tables S1-S2, References 39-55). This work was supported by the European Research Council (to S.J. and F.H.), the Swiss National Science Foundation (BSCGI0_157859 to S.J.), the Zurich Neuroscience Center, and the Wellcome Trust (098357/Z/12/Z to B.D.S.). G.A.P. was supported by an EMBO Long-Term Fellowship, M.B. by a SystemsX transition postdoc fellowship. We thank S. April for help with analyzing R cell morphology, D.L. Moore and D.C. Lie for comments on the manuscript. G.A.P. developed the imaging approach, performed imaging, analyzed data, and co-wrote the manuscript. S.B. performed imaging, analyzed data, and revised the manuscript. S.C. co-developed the imaging approach and performed imaging. M.B. analyzed data and revised the manuscript. D.J.J. and B.D.S. contributed to the concept, performed theoretical modelling, and co-wrote the manuscript. F.H. contributed to the concept and revised the manuscript. S.J. developed the concept and wrote the manuscript.

Figure legends:

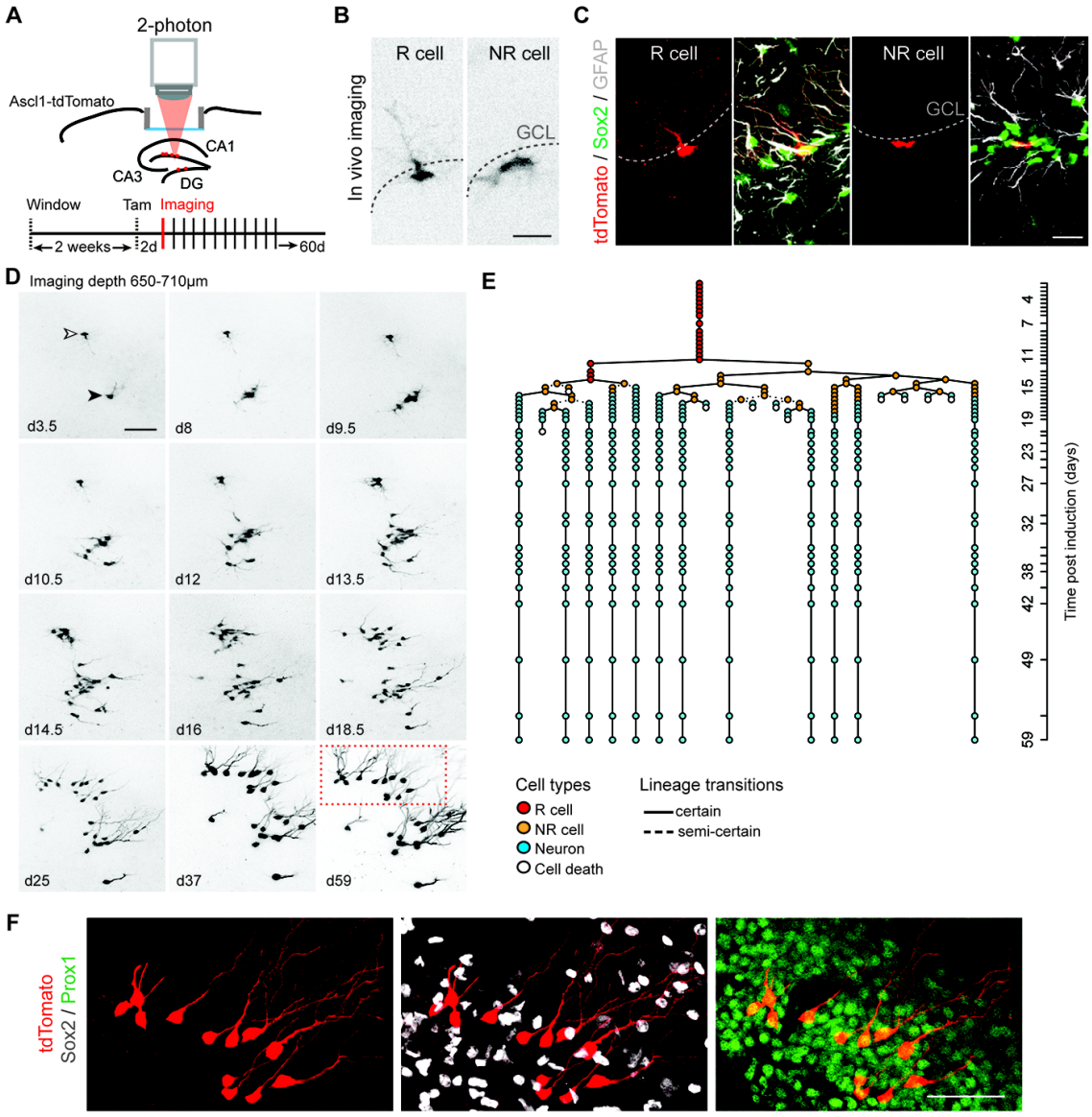

Fig. 1. Chronic *in vivo* imaging of neurogenesis in the adult DG.

(A) Scheme illustrating the experimental approach allowing for chronic *in vivo* imaging of NSPCs in the adult DG using Ascl1-tdTomato mice. (B) Representative *in vivo* imaging pictures of R and NR cells at 2 days post-induction (dpi). (C) Immunostained

images depicting Sox2-positive (green), Ascl1-tdTomato-labeled (red) R cells with GFAP-positive (white) radial processes and NR cells (Sox2-positive/GFAP-negative) in Ascl1-tdTomato mice at 2dpi. (D) Selected imaging time points of two R cells (depicted with open and closed arrowhead) over the course of 2 months resulting in two neuronal clones. Time points after Tam injection are indicated in each panel (d, days). Shown are collapsed z-stacks. Note the clonal expansion of individual R cell progeny and subsequent neuronal maturation. (E) Lineage tree deduced from tracking one R cell (open arrowhead in D) and its progeny. Cell types identified are color-coded and lineage transitions are depicted depending on their certainty (see Methods). Each circle in the lineage tree represents an imaging time point. Y axis shows the duration of the imaging (d, days). (F) *Post hoc* immunhistochemical analyses of the clone shown in D (boxed area at d59) confirm neuronal progeny with newborn cells positive for Prox1 (green) and negative for Sox2 (white). Note that the horizontal view of the DG corresponds to the view obtained during *in vivo* imaging.

Scale bars represent 20µm (A, B) and 50µm (C, D). GCL, granule cell layer.

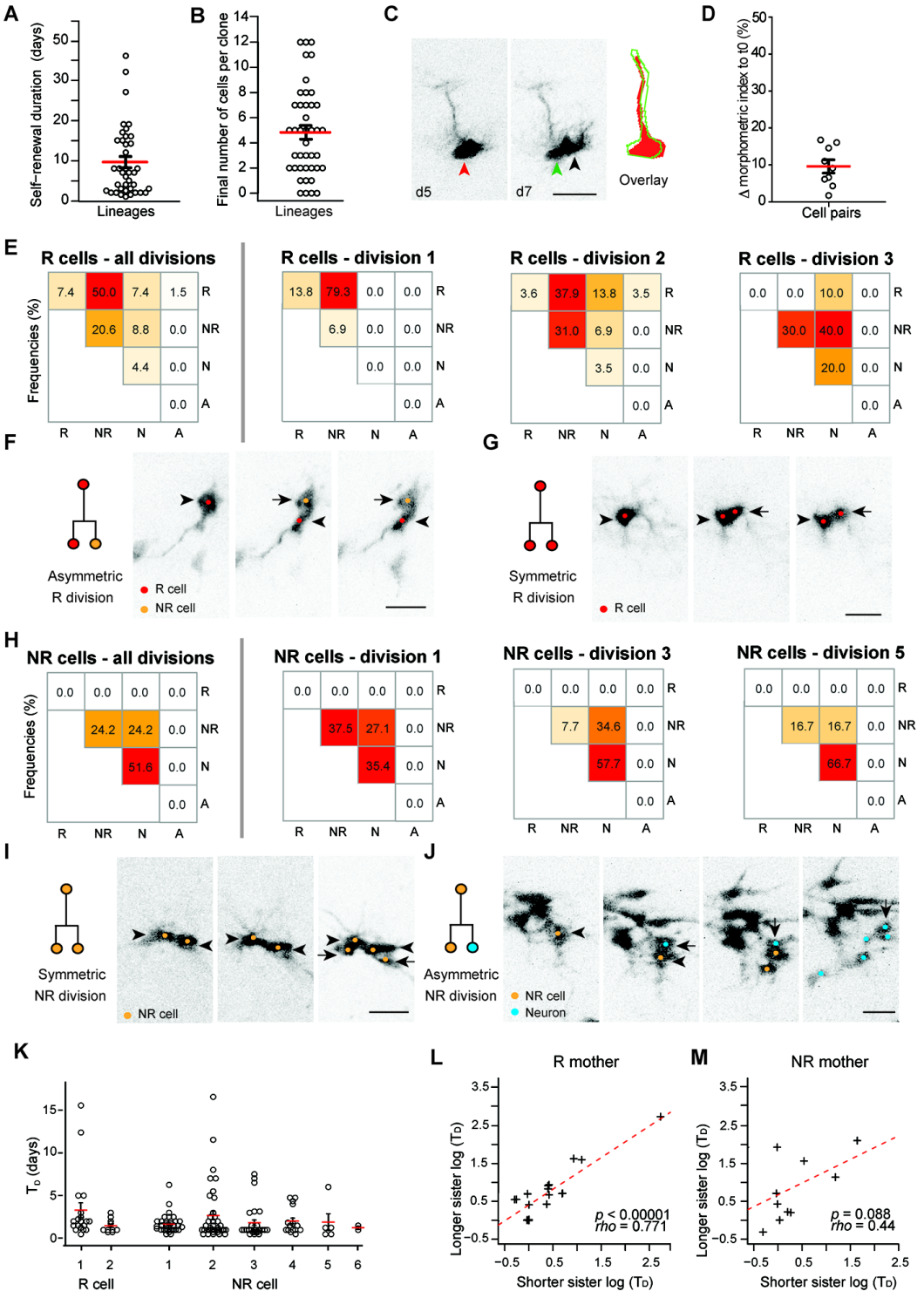

Fig. 2. The mode of NSPC division is associated with individual cell division history.

(A) Dot plot indicating the self-renewal duration (time between first and last division in each lineage) of R cells (9.6 ± 1.3 days; *n* = 39). (B) Distribution of the final number of

cells per active clone (n = 42 lineages). Open circles represent individual clones. (C) Chronic *in vivo* imaging before and after cell division illustrates asymmetric cell division of R cells. Note the large overlap with regards to the cellular morphology before (red arrowhead and red outline) and after R cell division (green arrowhead and green outline). Black arrowhead points at the asymmetrically generated daughter cell. (D) A morphometric index (MMI, including circularity and process length, see Methods for details) shows little deviation of cell morphology before and after cell division (9.6 ± 1.8%; n = 9). (E) Heat map representing the frequencies for modes of division of R cells (all divisions and division rounds 1-3; n = 68 divisions total). Note the change from a predominantly asymmetric (division 1) to a more symmetric differentiation (divisions 2, 3) division mode. (F) Example for an asymmetric division of an R cell. R cell is depicted with an arrowhead, daughter cell with an arrow (lineage 40, Fig. S3). (G) Example of a symmetric division of an R cell. Mother cell is depicted with an arrowhead, daughter cell with an arrow (lineage 13). (H) Heat map representing the frequencies for cell division modes of NR cells (all divisions and division round 1, 3 and 5; n = 153 divisions). (I) Image sequence showing symmetric NR division. Mother cell is depicted with an arrowhead, daughter cell with an arrow (lineage 1). (J) Example for an asymmetric division of a NR cell. Mother cell is depicted with an arrowhead, daughter cell with an arrow. Note that the NR daughter continues to divide (lineage 3). (K) Cell division time (T_D) of R cells and NR cells for different divisions. (L) The time until next cell division of sister cells originating from a single R mother cell are correlated (rho = 0.77; $*p < 0.00001$; Pearson correlation, n = 22 pairs). (M) The T_D of sister cells originating from a

single NR mother are not correlated (*rho* = 0.44; Pearson correlation, $p = 0.08$; $n = 16$ pairs).

Red lines represent means, black lines represent s.e.m. Scale bars represent 20μm (C, F, G, I, J).

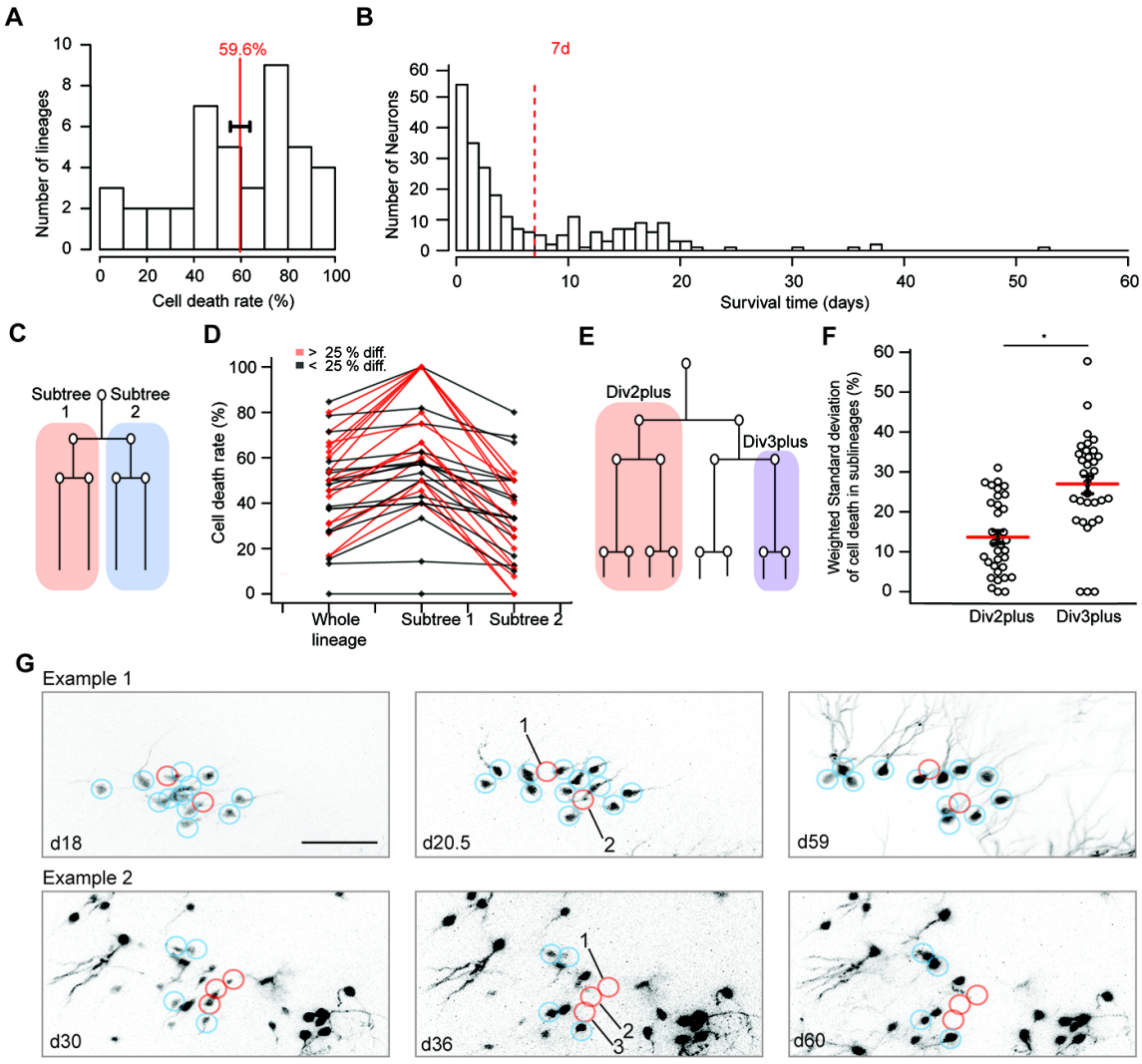

Fig. 3. Chronic *in vivo* imaging reveals variable susceptibility for cell death.

(A) Frequency of cell death in all chronically imaged lineages ranges from 0-100% (mean 59.6%, n = 42). (B) Shown is the time point of cell death after last cell division. Note the two peaks of cell death before and after 7 days with almost no cell death occurring > 20 days after birth (n = 242). (C) Pictogram depicting the comparison of cell death frequencies in subtree 1 and 2 derived after initial R cell division plus subsequent progeny within that subtree (Div2plus). (D) Plot showing the difference in cell death frequencies in subtree 1 and 2 in comparison with the cell death frequency in the whole

lineage (lineages with >25% difference in cell death rate are colored red; only early cell death until day 7 after birth was included). (E) Pictogram depicting the comparison of cell death frequencies in subtrees derived from the 2nd division after initial R cell division plus subsequent progeny within that subtree (Div3plus) compared to the Div2plus (see C) subtrees. (F) Cell death frequencies are more asymmetrically distributed among sublineages of Div3plus compared to Div2plus, as demonstrated by the higher weighted standard deviation to the Div2plus subtree death frequency (Div2plus difference: 13.6 ± 1.6; $n = 34$, Div3plus difference: 27 ± 2.2; $n = 33$; $*p < 0.0001$, Wilcoxon rank sum test). Weighted standard deviation was used to account for differences in subtree sizes within each clone. Red line represents mean, vertical lines represent s.e.m. (G) Shown are the locations of surviving newborn neurons (blue circles) relative to cells that underwent cell death (red circles). The observed death (calculated from birth of cell) for dying cells are 2.5d (cell 1, 2; example 1), 13d, 3d, 4d (cell 1, 2 and 3; example 2). Note the overlapping spatial localizations of surviving and dying cells.

Scale bar represents 100μm.

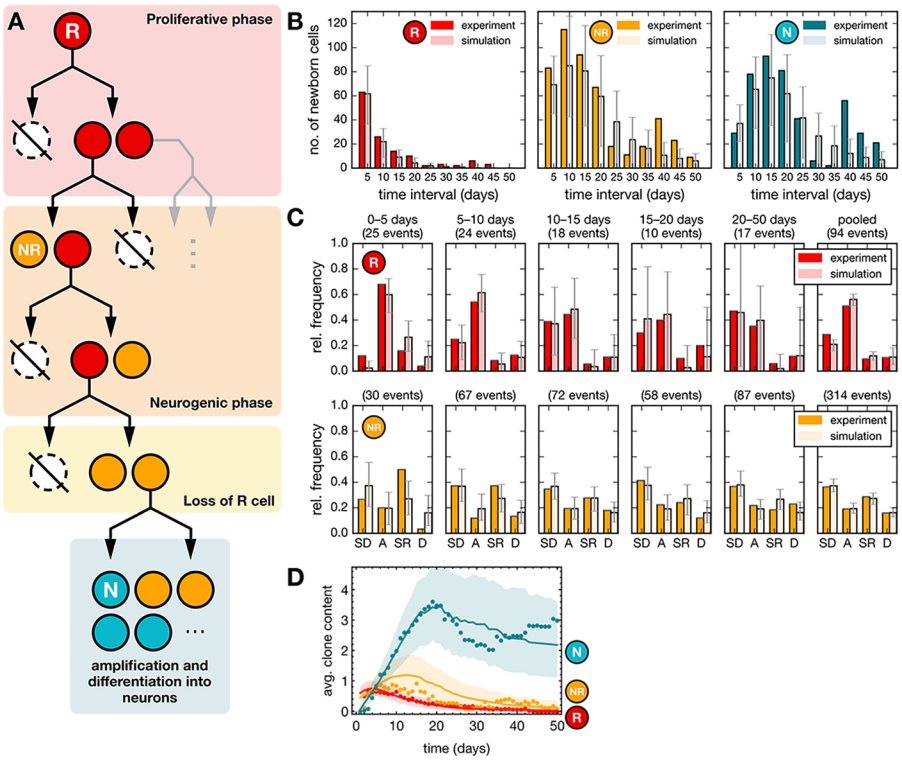

Fig. 4: Modelling-based analysis suggests a developmental-like program for R cell fate behavior.

(A) Model paradigm: R cells follow a defined program comprising a proliferative phase (duplications) that switches irreversibly into a neurogenic phase (asymmetric divisions and terminal differentiation). (B) Total number of newborn cells in successive time intervals of 5 days after induction from experiments (dark data set) and from simulations (bright dataset) for R and NR cells (see Methods). Cell counts have been pooled over 55 lineage trees with non-quiescent R cells and averaged over 500 realizations for each lineage tree resulting in a total of 27500 simulations (model parameters are given in Table S2). Error bars indicate the range within which 95% of the simulation results fall. (C) Relative frequencies of different cell fates in successive time intervals of 5 days after induction from experiments and simulations as in panel C. Later time intervals (20–50 days) with small numbers of events have been pooled together. (SD: symmetric

differentiating divisions, A: asymmetric divisions, SR: symmetric self-renewing divisions, D: cell death). (D) Average clone content as a function of time from experiments (dots) and from simulations (lines) for different cell types as indicated. Shaded areas indicate the regions within which 95% of the simulation results fall.